PCCP

Accepted Manuscript

ROYAL SOCIETY OF CHEMISTRY

www.rsc.org/pccp

Electronic structure aspects of the complete O_2 transfer reaction between Ni(II) and Mn(II) complexes with cyclam ligands

Jhon Zapata-Rivera,[a,b] Rosa Caballol*[a] and Carmen J. Calzado*[c]

[a] *Departament de Química Física i Inorgànica. Universitat Rovira i Virgili, Marcel·lí Domingo, s/n, 43007 Tarragona, Spain, caballol@urv.net*

[b] *Present address: Facultad de Ingeniería, Corporación Universidad de la Costa, calle 58 # 55-66, Barranquilla, Colombia, jzapatarivera@icloud.com*

[c] *Departamento de Química Física. Universidad de Sevilla, c/ Profesor García González, s/n, 41012 Sevilla, Spain. calzado@us.es*

Abstract

This work explores the electronic structure aspects involving the complete intermolecular O_2 transfer between Ni(II) and Mn(II) complexes, both containing N-tetramethylated cyclams (TMC). The energy of the low-lying states of reactants, intermediate and products is established at CASSCF level and also DDCI level when possible. The orthogonal valence bond analysis of the wave functions obtained from CASSCF and DDCI calculations indicates the dominant superoxide nature of all the adducts participating in the reaction, and consequently that the whole reaction can be described as the transfer of the superoxide O_2^- between Ni(II) and Mn(II) complexes, without any additional change on the electronic structure of the fragments.

Introduction

Biomimetic metal-oxygen complexes have been extensively described as key compounds for the understanding of the catalytic cycles of dioxygen activation by metalloenzymes.[1,2,3] The metal-O_2 adducts are also important in homogeneous and heterogeneous catalysis processes and many complexes containing different metal centers (Mn, Cu, Ni, Fe…) have been prepared and characterized as models of the reactive species. Beyond Cu complexes,[4] mononuclear LM-O_2 adducts are scarce, since they usually react fast to give $(LM)_2$-O_2 or higher nuclearity complexes, which in many cases are stable enough to be isolated and characterized. When reacting with other transition metal complexes, L'M', binuclear LM-O_2-L'M' complexes can be obtained, where the most frequent coordination modes are μ-η^2: η^2-O_2, bis(μ-O) and μ-η^1:η^1-O_2 in Cu, Ni, Mn, Fe and Co complexes.[5,6,7,8,9,10,11,12,13,14,15]

In contrast to the usual behaviour, Cho and coworkers[16] have recently described a novel reaction in which an intermolecular O_2-transfer occurs from a side-on Ni-O_2 complex to a Mn(II) one, both containing N-tetramethylated cyclams (TMC), and the products are the Ni(II) complex and the side-on Mn-O_2 adduct:

$$[(12\text{-TMC})\text{Ni-O}_2]^+ + [(14\text{-TMC})\text{Mn}]^{2+} \rightarrow [(12\text{-TMC})\text{Ni}]^{2+} + [(14\text{-TMC})\text{Mn-O}_2]^+ \quad (1)$$

where 12-TMC = 1,4,7,10-tetramethyl-1,4,7,10-tetraazacyclododecane and 14-TMC = 1,4,8,11-tetramethyl-1,4,8,11-tetraazacyclotetradecane.

The same authors indicate that a similar reaction occurs with the cobalt analogue $[(12\text{-TMC})\text{Co-O}_2]^+$, although in this case the reaction is ~1100 times slower.[17,18] These are the first-described complete O_2 transfer reactions between complexes bearing TMC ligands. The kinetic study performed at low temperature on the Ni-Mn system indicates a second order rate law, with first order on each reactant. The temperature dependence of the rate constant led to an activation enthalpy of $\Delta H^{\neq} = 11.7$ kcal·mol^{-1} and a negative activation entropy of $\Delta S^{\neq} = -18$ cal·mol^{-1}·K^{-1}. These data are compatible with a two-step mechanism, where the formation of the binuclear intermediate [(12-TMC)Ni-O_2-Mn[(14-TMC)]$^{3+}$ is supposed to be the rate-determining step, although this intermediate has not been isolated even at low temperature.

To elucidate the details of the mechanism favoring the complete O_2 transfer instead of the O_2-bridged dinuclear formation, we have recently carried out a theoretical study[19], where the stationary points of the low-lying potential energy surfaces (PES) compatible with the electronic states of the reactants have been located and

characterized. B3LYP calculations including long-range corrections and solvent effects support the experimentally proposed two-step mechanism and the formation of the intermediate in agreement with the kinetic studies.

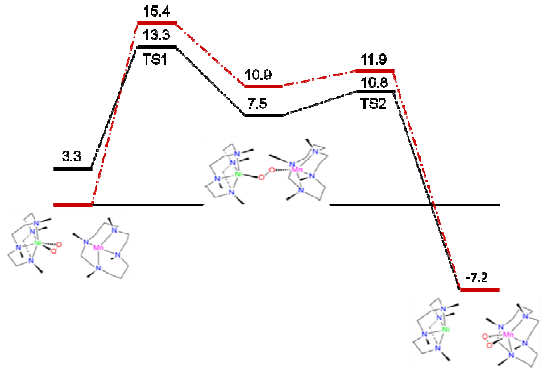

Figure 1. O_2 transfer mechanism from our B3LYP theoretical study[19]. BSSE corrected energies for the S = 1 (black) and S = 2 (red) pathways.

In the first step, the binuclear complex is formed, which rapidly dissociates to the products. The intermediate shows a μ-η^1:η^1 Ni-O-O-Mn core, a coordination mode present on few examples of dicopper, [12,13,20] dicobalt[14,21,22] and diiron[23] complexes. The transition states of both steps, TS1 and TS2, have been characterized. The ground state for TS1, TS2 and the intermediate is the triplet state, although only slightly stabilized with respect to the quintet state. The B3LYP reaction energy profile including BSSE corrections is shown in Figure 1.

Regarding the electronic structure of the adducts involved in the reaction, the $[(12\text{-TMC})Ni\text{-}O_2]^+$ and $[(14\text{-TMC})Mn\text{-}O_2]^+$ complexes have been both described as mononuclear metal-peroxo complexes by Cho and coworkers. This suggests the transfer of the peroxide O_2^{2-} accompanied by a change of the oxidation states of the metal centers to explain the reaction:

$$Ni(III)\text{-}O_2^{2-} + Mn(II) \rightarrow Ni(II) + Mn(III)\text{-}O_2^{2-} \qquad (2)$$

However, the analysis of the most relevant B3LYP natural orbitals of the optimized intermediate indicates that the O_2 moiety has a marked superoxide nature in the intermediate and also in the transition states. Then the reaction could be also interpreted as the migration of the superoxide O_2^- between the M(II) complexes:

$Ni(II)\text{-}O_2^- + Mn(II) \rightarrow Ni(II) + Mn(II)\text{-}O_2^-$ (3)

In fact, previous multiconfigurational CASSCF/CASPT2 and DDCI calculations[24] on the ground state of the $[(12\text{-TMC})Ni\text{-}O_2]^+$ complex indicate a dominant superoxide character for this complex (76% of $Ni(II)\text{-}O_2^-$ form), in contrast to the proposed peroxide structure. The peroxide character is not negligible, 8.1% of the $Ni(III)\text{-}O_2^{2-}$ form in the wave function, suggesting a superoxide-peroxide mixing.

It is the aim of this work to extend the study carried on the $[(12\text{-TMC})Ni\text{-}O_2]^+$ complex to the intermediate and products to gain a deeper understanding of the electronic effects accompanying the O_2 transfer between Ni and Mn complexes. As stated in the literature, the $LM\text{-}O_2$ complexes exhibit an intrinsic multiconfigurational character,[25] in such a way that the dynamical correlation effects are important to obtain a good description of the low-lying state energies and electronic structures. As in previous studies on related biomimetic complexes, we have used CASSCF and Difference Dedicated Configuration Interaction (DDCI) [26,27] calculations when possible to elucidate the electronic structure of the oxygenated species and the way in which the O_2 molecule is transferred from Ni to Mn complexes.

The results corroborate the preliminary sketch obtained from B3LYP natural orbitals. All the complexes containing dioxygen, reactant $[(12\text{-TMC})Ni\text{-}O_2]^+$, intermediate $[(12\text{-TMC})Ni\text{-}O_2\text{-}Mn[(14\text{-TMC})]^{3+}$ and product $[(14\text{-TMC})Mn\text{-}O_2]^+$, present a dominant superoxide nature, although with non-negligible contributions of the peroxide forms. Then in good approximation, the reaction can be described as just the migration of the superoxide unit between the metal centers, without the occurrence of a simultaneous intermolecular electron transfer.

Description of the complexes

To define the geometry of reactants and products we have used the available X-ray crystal structure data,[16,28] except for $[(14\text{-TMC})Mn]^{+2}$ for which the crystallographic data of $[(14\text{-TMC})Mn\text{-}Cl]^+$ have been employed.[29] As shown previously[19] B3LYP geometries when taking into account solvent and counterions are very close to the X-ray ones. For the intermediate, not yet isolated, the B3LYP optimized structure[19] has been used. In all the adducts, the O-O bond lengths are between those of the metal-superoxo compounds (~1.2–1.3 Å) and the metal-peroxo compounds (~1.4–1.5 Å). [30]

[(12-TMC)Ni-O_2]$^+$

The geometry of the [(12-TMC)Ni-O_2]$^+$ adduct has been built from the X-ray crystal data provided by Cho *et al.*[16] The complex structure belongs to the C_s point group (Figure 2), with a *side-on* 1:1 Ni-O_2 coordination, with both Ni and O_2 placed on the *yz* plane. The O-O and Ni-O average bond lengths are 1.386 Å and 1.889 Å, respectively. The axial Ni-N bond distances are slightly larger than the equatorial ones, in agreement with a tetragonal distortion along the *x* axis. The complex has been formulated by Cho *et al.*[16] as a Ni(III)-peroxo system based on the electron paramagnetic resonance, resonance Raman and Ni K-edge X-ray absorption spectra and X-ray crystal structure. A low spin ground state (S=1/2) is proposed for this adduct on the basis of the ^{1}H NMR Evans method.

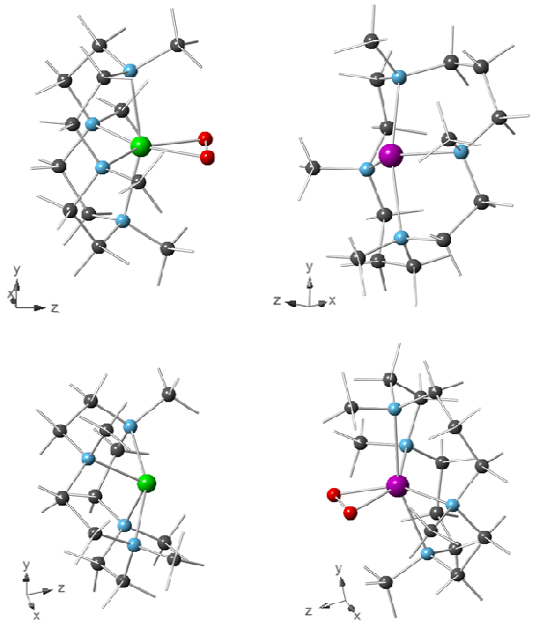

Figure 2. X-ray geometry of reactants (top) and products (bottom). Green, Ni; purple, Mn; red, O; blue, N; grey, C.

[(14-TMC)Mn-O_2]$^+$

The X-ray data by Seo *et al.*[28] have been used for the multiconfigurational calculations performed on [(14-TMC)Mn-O_2]$^+$ adduct, which structure belongs to the C_s point group (Figure 2). The O_2 molecule is symmetrically bound to the Mn ion in a *side-on*

coordination, where Mn and O_2 are situated on the *yz* plane. The O-O and Mn-O bond distances are 1.403 Å and 1.884 Å, respectively. Similarly to the $[(12\text{-TMC})Ni\text{-}O_2]^+$ adduct, the axial Mn-N bond distances are slightly larger than the equatorial ones, in agreement with a tetragonal distortion along the *x* axis. Although the O-O bond length is slightly shorter than in other Mn(III)-O_2 complexes,[31] as $[Mn(TPP)(\eta^2\text{-}O_2)]$,[32,33] and $[Mn(HB(3,5\text{-}iPr_2pz)_3)(3,5\text{-}iPr_2pzH)\ (\eta^2\text{-}O_2)]$,[33,34] ($d_{O\text{-}O}$ = 1.421 and 1.428 Å, respectively), Seo *et al.* proposed a Mn(III)-peroxo nature for this complex. The $[(14\text{-}TMC)Mn\text{-}O_2]^+$ is EPR silent but ^{1}H NMR data indicate a high spin state with S=2.

$[(12\text{-TMC})Ni\text{-}O_2\text{-}Mn(14\text{-TMC})]^{3+}$

Since the intermediate has not been isolated, we have used in this case the B3LYP optimized geometry of the cation in $Cl_3[(12\text{-TMC})Ni\text{-}O_2\text{-}Mn(14\text{-TMC})]$,[19] which belongs to the C_1 point group (Figure 3). The oxygen molecule binds in a $\mu\text{-}\eta^1\text{:}\eta^1$ coordination mode to Ni and Mn, forming a dihedral angle of 183.9°. This less-frequent coordination is probably due to the steric hindrance of the methyl groups in each of the macrocyclic ligands. The O-O, Ni-O and Mn-O bond lengths are 1.33 Å, 2.01 Å and 2.09 Å, respectively. The B3LYP calculations indicate a ground state with S=1.

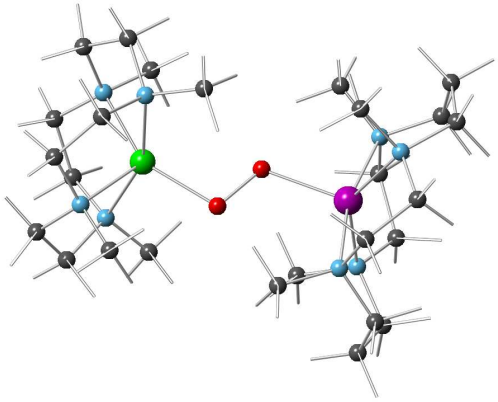

Figure 3. B3LYP optimized geometry of $[(12\text{-TCM})Ni\text{-}O_2\text{-}Mn(14\ TCM)]^{3+}$. Same color codes as in Figure 2.

$[(12\text{-TMC})Ni]^{+2}$ and $[(14\text{-TMC})Mn]^{+2}$

These complexes have deformed square pyramidal coordination, where the N atoms of the macrocyclic ligand define the pyramid base (Figure 2). No crystallographic data

have been published to our knowledge on [(14-TMC)Mn]$^{2+}$ and the XR structure of [(14-TMC)Mn-Cl]$^{+}$ has been used.[29] The Ni and Mn complexes present C_{2v} and C_2 symmetry, respectively. EPR data have not been given for [(12-TMC)Ni]$^{+2}$ but the complex has been proposed as a S=1 spin system, consistent with a high spin $3d^8$ configuration.[16]

Computational strategy

We have performed CASSCF and, when possible, DDCI calculations to analyze the electronic structure of the adducts. The active space has been rationally selected to reduce as far as possible the large computational demands of DDCI calculations. The complete set of CASSCF MOs (active, inactive occupied and virtual) has been localized. The localization of the inactive orbitals aims to reduce the cost of the DDCI calculations. In fact, the core orbitals of C, N, O and metal atoms (up to 3s), as well as the bonding and antibonding C-C and C-H orbitals have been frozen in the DDCI calculations, since they do not play a relevant role in the M-O_2 interaction, as shown previously. [19,35,36,37]

On the other hand, the localization of the active orbitals is seeking to provide and easier reading of the correlated multireference (MR) wavefunction, otherwise too complicate on the basis of delocalized MOs. The CAS projection of the MR wavefunction is written in terms of the orthogonal valence bond structures, giving a simplified chemical picture of the multiconfigurational character. We have previously used this strategy to analyze several LM-O_2 adducts with M = Cu, Ni,[37,**Error! Bookmark not defined.**38] but it has also been helpful in studying different kind of problems.[39-42] LM-O_2 delocalized active orbitals have a $3d\pm\pi^*$ nature. The localization of the active orbitals give almost pure 3d metal and O_2 π^* orbitals, in such a way that it is easy to calculate the relative weight of the three charge transfer forms between the metal M^{+n} ion and the O_2 molecule: peroxide $M^{+(n+2)}$ O_2^{-2}, superoxide $M^{+(n+1)}$ O_2^{-1}, and neutral M^{+n} O_2 forms. A similar scheme is obtained from the M-O_2-M' adducts. For the intermediate complex, where the DDCI calculations are not affordable, we have obtained a qualitative good description of the ground state at CASSCF level, followed by the Orthogonal Valence Bond (OVB) reading of the wave function.

Description of the Complete Active Space

[(12-TMC)Ni-O_2]$^+$. This adduct formally corresponds to the interaction of the [(12-TMC)Ni]$^+$ complex with O_2. The Ni(I) center has a $3d^9$ configuration, which gives a doublet state for the [(12-TMC)Ni]$^+$ fragment. The interaction of this doublet with the triplet state of the O_2 molecule can result in a doublet or in a quartet state. The active space contains the two O_2 π^* orbitals and all Ni 3d orbitals, a CAS (11,7).

[(14-TMC)Mn-O_2]$^+$. The electronic structure of this adduct can be analyzed as resulting from the interaction between [(14-TMC)Mn]$^+$ and O_2. Mn(I) is a $3d^6$ ion with a pseudooctahedral coordination, and the interaction of the Mn 3d with the two O_2 π^* singly occupied orbitals can lead to triplet, quintet and septet states of various symmetries. The active space contains eight electrons in seven orbitals, CAS(8,7), including the five Mn 3d and two O_2 π^* orbitals.

[(12-TMC)Ni-O_2-Mn(14-TMC)]$^{3+}$. This adduct can be split into three different fragments: (12-TMC)Ni(I), (14-TMC)Mn(II) and O_2. Ni(I) has a $3d^9$ configuration, while Mn(II) presents a high spin $3d^5$ configuration. The interaction of the metals with the O_2 π^* singly occupied orbitals leads to triplet, quintet or septet states. These electronic configurations suggest that the active space has to include sixteen electrons on the five 3d orbitals of Mn and Ni and the two O_2 π^* orbitals, CAS(16,12).

[(12-TMC)Ni]$^{+2}$ and [(14-TMC)Mn]$^{+2}$. In both complexes the oxidation state of the metal is formally M(II), which corresponds to $3d^8$ for Ni(II) and $3d^5$ for Mn(II). Hence, the active space contains the five 3d orbitals and eight and five electrons, respectively.

Computational details

In all calculations the relativistic with core correlation atomic natural orbital (ANO-RCC) basis sets have been used.[43,44] This basis set has shown good results in previous studies involving transition metal complexes.[25,45] For Ni and Mn, the [5s4p2d1f] contraction has been chosen. For atoms directly coordinated to the metal, O and N, the [4s3p1d] and [3s2p1d] contractions have been used, respectively. For atoms non-directly coordinated to the metal, C and H, the [3s2p] and [2s] contractions were used.

CASSCF and CASPT2 calculations have been performed by means of the MOLCAS 7.4 package, the latter using the the standard IPEA-modified zeroth order Hamiltonian H_0 (with a shift parameter IPEA of 0.25).[46] The molecular orbital localizations have been carried out with DOLO code[47] and the DDCI calculations with CASDI[48] suite of programs.

Electronic structure analysis

[(12-TMC)Ni]$^{+2}$ and [(14-TMC)Mn]$^{+2}$

CASSCF(5,5) calculations carried out on the Mn complex give ^{6}A as the ground state and ^{4}A as the first excited state, with a relative energy of 56 kcal·mol^{-1}. The orientation of the Cartesian axes is indicated in Figure 2.

In the case of the Ni complex, the ground state is the triplet $^3A_1$ in agreement with the experimental description. The two unpaired electrons occupy the $3d_{z2}$ and $3d_{x2-y2}$ orbitals. At the CASSCF(8,5) level, the two lowest excited states are both triplets of symmetry A_2 and B_1, separated by only 1.5 and 4.8 kcal·mol^{-1}, respectively, at this level of calculation.

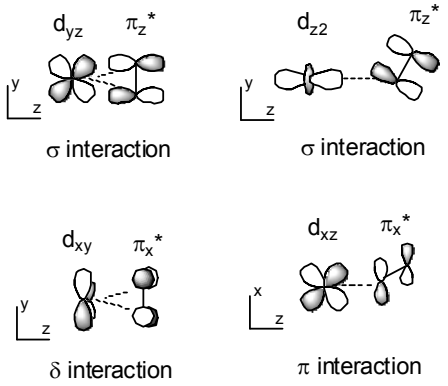

Scheme 1. σ-, π- and δ-interactions between the [(TCM)-M]$^+$ complex and O_2 in *side-on* (left) and *end-on* (right) coordination modes.

[12-TMC)Ni-O_2]$^+$

The electronic structure of the [12-TMC)Ni-O_2]$^+$ complex has been studied in deep in a previous work,[24] only the main findings are summarized here.

At the CASSCF(11,7) level, the ground state is ^{2}A', where the Ni $3d_{x2-y2}$ orbital

remains singly occupied as in the free complex, and two σ orbitals result from the bonding and anti-bonding $3d_{yz} \pm \pi_z^*$ combinations (Scheme 1). Two configurations have important weights, the largest one implying the bonding σ combination, $3d_{xy}^2\ \sigma^2\ \pi_x^{*2}\ 3d_{x2-y2}$ the other the anti-bonding σ* one, $3d_{xy}^2\ \sigma^{*2}\ \pi_x^{*2}\ 3d_{x2-y2}$. This gives occupations of 1.51 and 0.49 for the σ and σ* MOs. The $3d_{xz}$ and $3d_{z2}$ orbitals remain doubly occupied. This description is in agreement with the analysis provided by Cho *et al.*[16] based on the EPR spectrum.

The first excited state is a quartet, ^{4}A", only 6.3 kcal· mol^{-1} less stable than the ground state, containing three unpaired electrons on π_x^*, $3d_{yz}$ and $3d_{x2-y2}$ orbitals.

Since $3d_{xz}$ and $3d_{z2}$ Ni orbitals are doubly occupied, they have not been included in the active space employed in the DDCI calculations, to keep the whole CI space sizeable. Figure 4 shows the five orbitals that define the reference wave function at this correlated level. The ^{2}A' state was confirmed as the ground state, followed by ^{4}A", 8.8 kcal· mol^{-1} above.

The OVB analysis of the DDCI ground state wave function indicates weights of 84.4% of the superoxide, Ni(II)-O_2^-, and 9.0% of the peroxide, Ni(III)-O_2^{2-}, forms, in the CAS projection (see Table 1). These weights are very close to those extracted from the simple CASSCF (7,5) and CASSCF(11,7) wave functions. The external correlation slightly increases the weight of the neutral and peroxide forms by less than 3% and decreases the superoxide one by around 6%. However, the overall description is not changed.

Hence, the ground state can be described as a high spin Ni(II) ion, antiferromagnetically coupled with the O_2^- moiety. The peroxide character is not negligible and suggests a superoxide-peroxide mixing, consistent with the fact that the experimental O-O bond distance (1.386 Å) and O-O stretching frequency (1002 cm^{-1}) reported for this complex show values in between those considered as typical for superoxide (1.2-1.3 Å, 1050-1200 cm^{-1}) and peroxide (1.4-1.5 Å, 800-930 cm^{-1}) M-O_2 complexes. Nevertheless, the superoxide character is dominant, which is in contrast with the assignation given by Cho et al.[16]

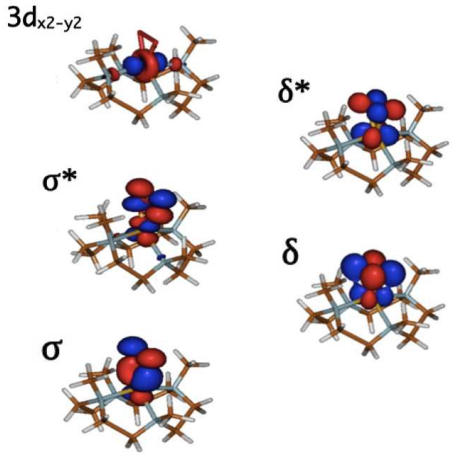

Figure 4. CASSCF(7,5) symmetry-adapted active orbitals of $[(12\text{-TMC})Ni\text{-}O_2]^+$ $^2A'$ ground state.

Table 1. $[(12\text{-TMC})Ni\text{-}O_2]^+$ ground state configurations weights (%) of the CASSCF(11,7), CASSCF(7,5) and DDCI(7,5) wave functions, in terms of charge transfer forms.

	CASSCF(11,7)	CASSCF(7,5)	DDCI(7,5)[a]
Ni(I)-O_2	3.7	3.5	6.6
Ni(II)-O_2^-	90.1	90.0	84.4
Ni(III)-O_2^{2-}	6.2	6.5	9.0

[a]CAS-projected DDCI wave function

$[(14\text{-TMC})Mn\text{-}O_2]^+$

Table 2 shows the relative energies of the lowest quintet and triplet states at CASSCF and CASPT2 levels for the $[(14\text{-TMC})Mn\text{-}O_2]^+$ complex. The septet states are too high in energy and have not been included.

Table 2. $[(14\text{-TMC})\ Mn\text{-}O_2]^+$ low-lying states CASSCF, CASPT2 and DDCI relative energies (kcal·mol^{-1}). A CAS(8,7) reference has been used in all the calculations.

State	CASSCF	CASPT2	DDCI
^3A	51.4	67.7	-
^3B	46.6	60.7	-
^5A	17.0	27.4	26.6
^5B	0.0	0.0	0.0

At all levels of calculation the ground state is the ^{5}B quintet. At the CASSCF level, the excited quintet ^{5}A is found 17.0 kcal·mol^{-1} above and the ^{3}A and ^{3}B triplet states are well separated, at 46.6 and 51.4 kcal·mol^{-1}, respectively. The CASPT2 relative energies show a similar trend although the dynamical correlation increases the relative energies by approximately 10-15 kcal·mol^{-1}.

Figure 5 shows some of the ^{5}B symmetry-adapted CASSCF(8,7) active orbitals. The Mn-O_2 bonding is due to the σ interaction between the Mn $3d_{yz}$ and O_2 π^*_z orbitals (Scheme 1). At this level, the occupations of the bonding and antibonding combinations of the $3d_{yz}$ and π^*_z orbitals, σ and σ*, are 1.67 and 0.33, respectively. The δ-type interaction between Mn $3d_{xy}$ and π^*_x O_2 orbitals is negligible, as expected from the steric hindrance of the methyl groups. In fact, these two orbitals practically do not mix, as shown in Figure 5. Hence, the orbital O_2 π^*_x carries two electrons, while the orbitals Mn $3d_{xy}$, $3d_{x2-y2}$, $3d_{xz}$ and $3d_{z2}$ are singly occupied. Three dominant configurations can be distinguished in the wave function of the quintet ground state, all them with two electrons in the σ and σ* orbitals:

(i) $\pi^*_x{}^2\ \sigma^2\ 3d_{xy}\ 3d_{x2-y2}\ 3d_{xz}\ 3d_{z2}$,

(ii) $\pi^*_x{}^2\ \sigma^{*2}\ 3d_{xy}\ 3d_{x2-y2}\ 3d_{xz}\ 3d_{z2}$ and

(iii) $\pi^*_x{}^2\ \sigma\ \sigma^*\ 3d_{xy}\ 3d_{x2-y2}\ 3d_{xz}\ 3d_{z2}$,

with weights of 77, 10 and 12%, respectively. These electronic configurations are consistent with a high-spin Mn ion in agreement with the interpretation provided by Seo et al.[28] based on the NMR data.

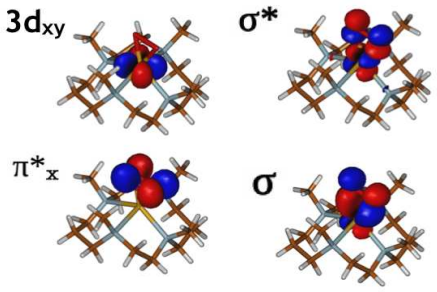

Figure 5. $[(14\text{-TCM})Mn\text{-}O_2]^+$ ground state symmetry-adapted active orbitals: (right) orbitals relevant to the Mn-O_2 bonding; (left) active orbitals essentially localized on Mn $3d_{xy}$ and O_2 π_x^* orbitals showing the negligible δ interaction between Mn and O_2.

The DDCI relative energies of the low-lying states are also reported in Table 2. All

DDCI calculations were performed on the basis of the averaged CASSCF MOs of the ^{5}A and ^{5}B states. These calculations confirm ^{5}A to be the first excited state, separated by 26.6 kcal·mol^{-1} from the ^{5}B ground state. As in the CASPT2 calculations, the DDCI external correlation favors the quintet ground state by about 10 kcal·mol^{-1}.

The DDCI wave function of the ground state has been analyzed on the basis of the OVB structures. The weight of the charge transfer forms of the ground state DDCI wave function are reported in Table 3. The projection onto the CAS of this wave function shows that the external correlation induces only small changes in the description with similar trends as in [(12-TCM)Ni-O_2]$^+$, with a slight increase of the peroxide weight and a slight decrease of the superoxide one. The DDCI wave function of the ground state (see Table 3) indicates a dominant superoxide nature, Mn(II)-O_2^-, where the leading configuration represented in Figure 6, reaches 77.3% of the CAS-projected DDCI wave function. The neutral form, Mn(I)-O_2, has only a weight of 3.1%. The peroxide form, Mn(III)-O_2^{2-}, suggested to be the main form by the experimental studies, has only a weight of 19.6% in the CAS-projected DDCI wave function. This weight is the largest found in all the systems analyzed using multiconfigurational methods[24,37,38] and indicates a non-negligible contribution of peroxide in the description of the electronic structure of the ground state, but is not in agreement with the rotund assignation as Mn(III)-peroxide. In fact, the OVB analysis of the DDCI wave function is consistent with a configuration containing a local sextet in Mn(II), with one unpaired electron on each of the Mn 3d orbital, antiferromagnetically coupled to the unpaired electron on O_2 π^*_z orbital. This electronic structure is in agreement with the NMR data suggesting a high-spin Mn(II) and a coordinated superoxide molecule.

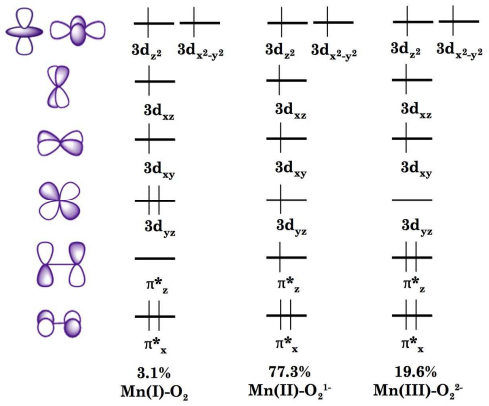

Figure 6. [(14TMC)Mn-O_2]$^+$ DDCI localized configurations for the ^{5}B state.

Table 3. $[(14\text{-TMC})Mn\text{-}O_2]^+$ ground state configuration weights (%) of the CASSCF(8,7) and DDCI(8,7) wave functions, in terms of charge transfer forms.

	CASSCF	DDCI[a]	DDCI leading configurations
Mn(I)-O_2	2.0	3.1	$\pi^*_x{}^2\ 3d_{yz}{}^2\ 3d_{xy}\ 3d_{x2-y2}\ 3d_{xz}\ 3d_{z2}$
Mn(II)-O_2^-	81.1	77.3	$\pi^*_x{}^2\ \pi^*_z\ 3d_{yz}\ 3d_{xy}\ 3d_{x2-y2}\ 3d_{xz}\ 3d_{z2}$
Mn(III)-O_2^{2-}	16.9	19.6	$\pi^*_x{}^2\ \pi^*_z{}^2\ 3d_{xy}\ 3d_{x2-y2}\ 3d_{xz}\ 3d_{z2}$

[a] CAS-projected DDCI wave function

$[(12\text{-TMC})Ni\text{-}O_2\text{-}Mn(14\text{-TMC})]^{3+}$

The size of this system makes the DDCI calculation unaffordable even with a substantial truncation of the inactive MOs subset, since the main bottleneck is the size of the reference space, with sixteen electrons distributed in ten 3d orbitals and two □* orbitals. However, it is possible to obtain a qualitative picture of the electronic structure at the CASSCF level, presumably not very different to the correlated picture as previously shown for the $[12\text{-TMC})Ni\text{-}O_2]^+$ and $[(14\text{-TMC})Mn\text{-}O_2]^+$ complexes.

As stated before CASSCF(16,12) calculations have been performed in this adduct, and a ^3A ground state is found. The quintet ^5A and septet ^7A are practically degenerate, at only 0.2 and 0.5 kcal·mol^{-1} above the ground state. This relative distribution of the low-lying states is consistent with the previously found from B3LYP calculations.[19] The most relevant ground state delocalized CASSCF active orbitals are represented in Figure 7. The Ni $3d_{xz}$, $3d_{yz}$ and $3d_{xy}$ orbitals maintain a double occupation, as well as the O_2 π^*_z orbital. In fact, the same description and relative stability of the low-lying states are obtained with a CAS(10,9), containing the five Mn 3d orbitals, the two O_2 π^* orbitals and only Ni $3d_z{}^2$ and $3d_{x^2-y^2}$.

We have analyzed the CASSCF(10,9) wave function of the triplet state to determine the degree of charge transfer between both metals, if any, and to figure out the oxidation state of Mn, Ni and O_2 in the intermediate. There exists a π-type interaction (Scheme 1) between the Mn $3d_{xz}$ and the O_2 π^*_x orbitals (Figure 7). The bonding and antibonding combinations of these two orbitals present occupations of 1.1 and 0.9, respectively. The

O_2 π^*_z orbital is doubly occupied and the remaining Ni and Mn 3d active orbitals are practically singly occupied. In both states the σ and δ interactions between the metal atoms and O_2 are nearly null.

An OVB analysis of the CASSCF wave function has been done on the basis of the localized active orbitals of the ^{3}A state. Table 4 shows the configurations and the weight of the charge transfer forms. The superoxide form, Ni(II)-O_2^--Mn(II), with a weight of 98%, governs the triplet state. The Ni(II)-O_2^- moiety maintains the [(12-TMC)Ni-O_2]$^+$ superoxide, but the occupation of the orbitals is modified with the deformation of the Ni-O-O angle and the consequent stabilization of the quartet with respect to the doublet in this fragment compatible with the [(12-TMC)Ni-O_2-Mn(14-TMC)]$^{3+}$ triplet state, as discussed previously.[19] This configuration, where Ni(II) has a local triplet and Mn(II) a local sextet, is shown in Figure 8. All the remaining configurations, have very small weights not higher than 1%. The Ni(II)-O_2^{2-}-Mn(III) configuration is the major contribution to the very small weight of the peroxide form. Although this description is obtained at the CASSCF level, it is expected that the dynamical correlation only modifies slightly the relative weights of the different charge transfer forms, but not the general trend, as for the adducts of Mn and Ni.

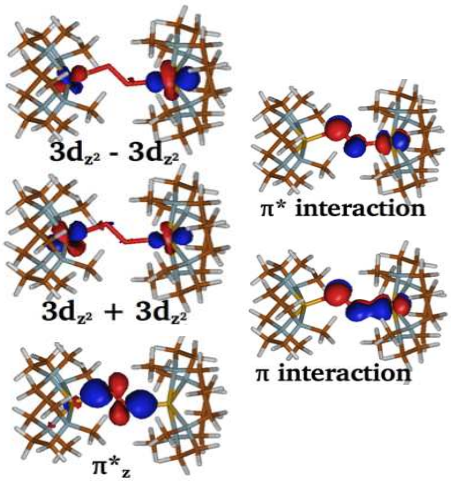

Figure 7. [(12-TMC)Ni-O_2-Mn(14-TMC)]$^{3+}$ ground state symmetry-adapted active orbitals relevant to the Ni-O_2-Mn interaction.

The electronic structure of the quintet ^{5}A is quite similar, with a marked dominant superoxide form. The dominant configurations in the analyzed states are consistent with both metallic centers in high-spin states, i.e., a local triplet in Ni(II) and a local sextet in

Mn(II), which are coupled in an antiferromagnetic manner. The so-resulting quartet can be coupled ferromagnetically or antiferromagnetically with the unpaired electron on the π^*_x orbital of O_2^-, giving the quintet or triplet states of the intermediate. At this level, we do not observe the formation of the peroxide on the intermediate, but only the formal transfer of one electron from Ni(I) to O_2.

The description resulting from these CASSCF calculations is consistent with that provided by our previous B3LYP calculations.[19] The analysis of the ground state natural orbitals gave single occupations of two Ni and five Mn 3d orbitals and three electrons occupying the two π^* orbitals of the O_2, consistent with an O_2 spin population of -0.99 and a dominant superoxide Ni(II)-O_2^--Mn(II) electronic configuration.

Table 4. [(12-TMC)Ni-O_2-Mn(14-TMC)]$^{3+}$ triplet configuration weights (%) of the CASSCF(10,9) wave function in terms of charge transfer forms.

CT form	^{3}A	Ni	O_2	Mn
Ni(II)-O_2^--Mn(II)	98	$3d_{x2-y2}3d_{z2}$	$\pi^*_x\pi^{*2}_z$	$3d_{yz}3d_{xy}3d_{x2-y2}3d_{xz}3d_{z2}$
Ni(I)-O_2-Mn(II)	1	$3d_{x2-y2}3d_{z2}^2$	$\pi^*_x\pi^*_z$	$3d_{yz}3d_{xy}3d_{x2-y2}3d_{xz}3d_{z2}$
Ni(II)-O_2^{2-}-Mn(III)	1	$3d_{x2-y2}3d_{z2}$	$\pi^{*2}_x\pi^{*2}_z$	$3d_{yz}3d_{xy}3d_{x2-y2}3d_{z2}$

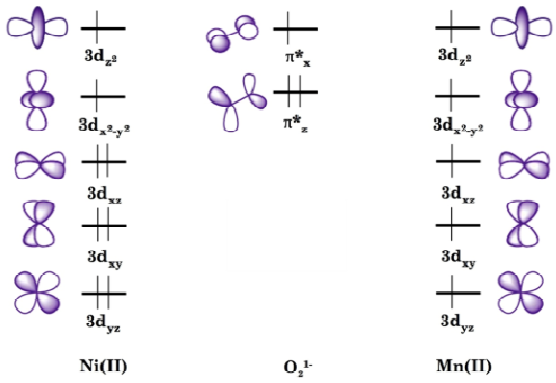

Figure 8. [(12-TMC)Ni-O_2-Mn(14-TMC)]$^{3+}$ largest contribution configuration (98%) in terms of localized orbitals for the ^{3}A state of the intermediate.

Discussion and conclusions

Once the ground state of all the involved species has been established, let us take a look at the global process. In the reaction, the $[(12\text{-TMC})Ni\text{-}O_2]^+$ complex, with a doublet ground state, interacts with the $[(14\text{-TMC})Mn]^{+2}$ complex in the sextet ground state. This gives a quintet as the ground state for reactants. However, the excited triplet state is close enough to make possible an alternative pathway through the S=1 potential energy surface, compatible with the triplet ground state of the intermediate. This excited S=1 state comes from the interaction between the local excited $[(12\text{-TMC})Ni\text{-}O_2]^+$ triplet and the ground sextet $[(14\text{-TMC})Mn]^{+2}$ states.

In fact, at CASSCF(11,7) level, the quartet state of the $[(12\text{-TMC})Ni\text{-}O_2]^+$ complex is 6.3 kcal·mol^{-1} above the ground state at the optimal *side-on* coordination. To bind the Mn complex, the Ni-O_2 *side-on* geometry must evolve to an *end-on* coordination, to release one of the O atom and bind the Mn center in a $\mu\text{-}\eta^1\text{:}\eta^1$ Ni-O_2-Mn arrangement. The Ni-O_2 deformation goes with the stabilization of the quartet state in front of the doublet state.[38] CASSCF(11,7) calculations of both the doublet and the quartet states of the distorted $[(12\text{-TMC})Ni\text{-}O_2]^+$ confirm the inversion of the relative position of these two states. At the geometry adopted by this fragment in the transition state TS1, with an open Ni-O-O angle enabling the formation of the O-Mn bond, the quartet is the ground state, 0.5 kcal·mol^{-1} more stable than the doublet state.

The $[(12\text{-TMC})Ni\text{-}O_2]^+$ dominant configuration for the quartet state in the distorted geometry is $3d_{xz}^2\ 3d_{xy}^2\ (3d_{yz} + 3d_{z2})^2\ \pi_z^{*2}\ \pi_x^*(3d_{yz} - 3d_{z2})\ 3d_{x2-y2}$. This is essentially the same configuration found for the $[(12\text{-TMC})Ni\text{-}O_2]^+$ fragment on the intermediate. Hence, the distortion induces a mixing of the Ni $3d_{yz}$ and $3d_{z2}$ orbitals, moving the unpaired electron from $3d_{yz}$ in the quartet state of the *side-on* Ni-O_2 to the $3d_{z2}$ in the ground state of the $\mu\text{-}\eta^1\text{:}\eta^1$ intermediate.

The interaction of this fragment with the five open shells of the Mn(II) complex in the intermediate does not introduce any additional change on the electronic configuration. According to the dominant configuration of the triplet ground state, no electron transfer between the fragments is observed, neither between Mn and O_2 nor between the metal centers. Hence, the intermediate keeps the superoxide nature, i.e. the Ni(II)-O_2^--Mn(II) form. Finally, the Ni-O bond cleaves to produce the $[(12\text{-TMC})Ni]^{+2}$ complex, with two unpaired electrons on $3d_{x2-y2}$ and $3d_{z2}$ coupled in a triplet ground state, and $[(14\text{-TMC})Mn\text{-}O_2]^+$, with a quintet ground state. The Mn-O_2 complex shows a

distorted *end-on* coordination immediately after overcoming the transition state conducting to products. This complex finally evolves to a more stable *side-on* Mn-O_2 coordination.

The reaction can be understood as the sum of the two following partial reactions:

[(12-TMC)Ni(II) -O_2^-] + [(14-TMC)Mn(II)]

→ [(12-TMC)Ni(II)-O_2^--Mn(II)(14-TMC)] (4a)

[(12-TMC)Ni(II)-O_2^--Mn(II) (14-TMC)]

→ [(14-TMC)Mn(II)-O_2^-] + [(12-TMC)Ni(II)] (4b)

In contrast with the experimental interpretation, that suggest the transfer of the peroxide molecule, the electronic structures of reactant, intermediate and products are consistent with the migration of the superoxide molecule from the Ni(II) to the Mn(II) complexes, without any additional change on the electronic structure of the fragments.

This study puts in evidence the marked multiconfigurational nature of the adducts resulting from the bonding between the dioxygen molecule and Ni and Mn complexes. This multiconfigurational character can be caught at CASSCF level, with only small and not relevant differences when the dynamical correlation is also taken into account, as proved by the DDCI calculations performed on Ni-O_2 and Mn-O_2 complexes. The main effect of the dynamical correlation is to modify to a small extent the energy of the low-lying states, but not their relative distribution. The analysis of the ground state wavefunction on the basis of the localized active orbitals and in terms of the charge transfer forms supplies a clear picture of the dominant configuration on each system, and the relative weight of the superoxide and peroxide forms. The fact that the O-O distances and O-O stretching frequencies reported for these complexes show values in between those considered as typical for superoxide and peroxide M-O_2 complexes support the superoxide/peroxide mixing resulting from our calculations. For the intermediate, not yet isolated, it is not possible to compare with experimental data, only to predict a ground state where the superoxide O_2^- bridges the Ni(II) and Mn(II) complexes, in agreement with the electronic structure found for the reactants and products of this reaction.

In summary, this work emphasizes the potential complementarities between the experimental findings and the theoretical calculations in order to enhance and extend the knowledge about the electronic aspects of the reactivity of these biomimetic metal-

dioxyen adducts.

Acknowledgments

Financial support has been provided by the Spanish Administration (Projects CTQ2011-23140 and CTQ2009-07767), the Generalitat de Catalunya (Project 2014SGR199 and Xarxa d'R+D+I en Química Teòrica i Computacional, XRQTC) and the European Union (COST Action CODECS CM1002). J.Z.R. acknowledges the Asociación Universitaria Iberoamericana de Postgrado (AUIP) for a mobility grant at the Universidad de Sevilla (Spain). The Supercomputing Team of the Centro Informático Científico de Andalucía (CICA) is acknowledged for the technical support.

1 E. I. Solomon, U. M. Sundaram, T. E. Machonkin, *Chem. Rev*., 1996**, 96**, 2563.

2 N. Kitajima, Y. Moro-Oka, *Chem. Rev*., 1994, **94**, 737.

3 E. I. Solomon, D. E. Heppner, E. M. Johnston, J. W. Ginsbach, J. Cirera, M. Qayyum, M. T. Kieber-Emmons, C. H. Kjaergaard, R. G. Hadt and L. Tian, *Chem. Rev.*, 2014, **114**, 3659.

4 L. M. Mirica, X. Ottenwaelder, T. D. P. Stack, *Chem. Rev*., 2004, **104**, 1013.

5 M. U. Triller, W.-Y Hsieh, V. L. Pecoraro, A. Rompel, B. Krebs, *Inorg. Chem.*, 2002, **41**, 5544.

6 J. Glerup, P. A. Goodson, A. Hazell, R. Hazell, D. J. Hogdson, C. J. McKenzie, K. Michelsen, U. Rychlewska, H. Toftlund, *Inorg. Chem.*, 1994, **33**, 4105.

7 H. Kang, J. Cho, K.-B. Cho, T. Nomura, T. Ogura, W. Nam, *Chem. Eur. J*., 2013, **19**, 14119.

8 K. Shiren, S. Ogo, S. Fujinami, H. Hayashi, M. Suzuki, A. Uehara, Y. Watanabe, Y. Moro-Oka, *J. Am. Chem. Soc.*, 2000, **122**, 254.

9 S. Hikichi, M. Yoshizawa, Y. Sasakura, M. Akita, Y. Moro-oka, *J. Am. Chem. Soc*., 1998, **120**, 10567.

10 L. Que, Jr., W. B. Tolman, *Angew. Chem., Int. Ed.*, 2002, **41**, 1114.

11 H.-F. Hsu, Y. Dong, L. Shu, V. G. Young, Jr., L. Que, Jr., *J. Am. Chem. Soc*., 1999, **121***,* 5230.

12 K. Komiyama, H. Furutachi, S. Nagatomo, A. Hashimoto, H. Hayashi, S. Fujinami, M. Suzuki, T. Kitagawa, *Bull. Chem. Soc. Jpn.*, 2004, **77**, 59.

[13] C. Würtele, O. Sander, V. Lutz, T. Waitz, F. Tuczek, S. Schindler, *J. Am. Chem. Soc.*, 2009, **131**, 7544.

[14] R. M. Hartshorn, S. G. Telfer, *J. Chem. Soc., Dalton Trans.*, 2000, 2801.

[15] E. E. Chufán, S. C. Puiu, K. D. Karlin, *Acc. Chem. Res*., 2007, **40**, 563.

[16] J. Cho, R. Sarangi, J. Annaraj, S. Y. Kim, M. Kubo, T. Ogura, E. I. Solomon, W. Nam, *Nature Chem.*, 2009, **1**, 568.

[17] J. Cho, R. Sarangi, H. Y. Kang, J. Y. Lee, M. Kubo, T. Ogura, E. I. Solomon, W. Nam. *J. Am. Chem. Soc.*, 2010, **132**, 16977.

[18] J. Cho, R. Sarangi, W. Nam, *Acc. Chem. Res*., 2012, **45**, 1321.

[19] J. Zapata-Rivera, R. Caballol, C. J. Calzado, D. G. Liakos, F. Neese, *Chem Eur. J.*, 2014,**20**, 13296.

[20] R. R. Jacobson, Z. Tyeklar, A. Farooq, K. D. Karlin, S. Liu, J. Zubieta, *J. Am. Chem. Soc.*, 1988, **110**, 3690.

[21] S. Fallab, M. Zehnder, *Helv. Chim. Acta*, 1984, **67**, 392.

[22] T. Tanase, T. Onaka, M. Nakagoshi, I. Kinoshita, K. Shibata, M. Doe, J. Fujii, S. Yano, *Chem. Commun.*, 1997, 2115.

[23] J. P. Collman, A. Dey, Y. Yang, S. Ghosh, R.A. Decréau, *Proc. Natl Acad. Sci. USA*, 2009, **106**, 10528.

[24] J. Zapata-Rivera, R. Caballol, C. J. Calzado, *J. Comput. Chem*., 2012, **33**, 1407.

[25] S. M. Huber, A. R. M. Shahi, F. Aquilante, C. J. Cramer, L. Gagliardi, *J. Chem. Theory Comput.*, 2009, **5**, 2967.

[26] J. Miralles, J.-P. Daudey, R. Caballol, *Chem. Phys. Lett.*, 1992, **198**, 555.

[27] J. Miralles, O. Castell, R. Caballol, J.-P. Malrieu, *Chem. Phys.*, 1993, **172,** 33.

[28] M. S. Seo, J. Y. Kim, J. Annaraj, Y. Kim, Y.-M. Lee, S.-J. Kim, J. Kim, W. Nam, *Angew. Chem., Int. Ed.*, 2007, **46**, 377.

[29] C. Bucher, E. Duval, J.-M. Barbe, J.-N. Verpeaux, C. Amatore, R. Guilard, L. Le Pape, J.-M. Latour, S. Dahaoui, C. Lecomte, *Inorg. Chem*., 2001, **40**, 5722.

[30] C. J. Cramer, W. B. Tolman, K. H. Theopold, A. L. Rheingold, *Proc. Natl Acad. Sci. USA,* 2003, **100**, 3635.

[31] V. L. Pecoraro, M. J. Baldwin, A. Gelasco, *Chem. Rev.*, 1994, **194**, 807.

[32] R. B. VanAtta, C. E. Strouse, L. K. Hanson, J. S. Valentine, *J. Am. Chem. Soc.*, 1987, **109**, 1425.

[33] Abbreviations: TPP = tetraphenylporphyrin; HB(3,5-iPr2pz)3 = hydrotris(3,5-diisopropyl-1-pyrazolyl)borate; 3,5-iPr2pzH = 3,5-diisopropylpyrazole.

[34] N. Kitajima, H. Komatsuzaki, S. Hikichi, M. Osawa, Y.Moro-oka, *J. Am. Chem. Soc.*, 1994, **116,** 11596.

[35] D. Maynau, S. Evangelisti, N. Guihery, J.-P. Malrieu and C. J. Calzado, *J. Chem. Phys.*, 2002, **116**, 10060.

[36] C. Angeli, S. Evangelisti, R. Cimiraglia and D. Maynau, *J. Chem. Phys.*, 2002, **117**, 10525.

[37] J. Zapata-Rivera, R. Caballol and C. J. Calzado, *Phys. Chem. Chem. Phys*. 2011, **13**, 20241.

[38] J. Zapata-Rivera, R. Caballol, C.J. Calzado, . *J. Comput. Chem*. 2011, **32**, 1144.

[39] J.P. Malrieu, N. Guihéry, C.J. Calzado, C. Angeli, *J. Comput. Chem.* 2007, **28**, 35.

[40] C. Angeli, *J. Comput. Chem*. 2009, **30**, 1319.

[41] C. Angeli, C.J. Calzado, C. de Graaf, R. Caballol, *Phys. Chem. Chem. Phys*. 2011, **13**, 14617.

[42] M. Kepenekian, V. Vetere, B. Le Guennic, P.Maldivi, V. Robert, *Chem. Eur. J.* 2011, **17**, 12045.

[43] B. O. Roos, *Mol. Phys.* 2003, **101**, 87.

[44] B. O. Roos, R. Lindh, P.-Å. Malmqvist, V. Veryazov, P.-O. Widmark, *J. Phys. Chem. A*, 2005, **109**, 6575.

[45] N. W. Aboelella, S. V. Kryatov, B. F. Gherman, W. W. Brennessel, V. G. Young, Jr., R. Sarangi, E. V. Rybak-Akimova, K. O. Hodgson, B. Hedman, E. I. Solomon, C. J. Cramer, W. B. Tolman, *J. Am. Chem. Soc.*, 2004, **126,** 16896.

[46] F. Aquilante, L. de Vico, N. Ferré, G. Ghigo, P.-Å. Malmqvist, P. Neogrady, T. B. Pedersen, M. Pitoňák, M. Reiher, B. O. Roos, L. Serrano-Andrés, M. Urban, V. Veryazov, R. Lindh, *J. Comput. Chem.*, 2010, **31**, 224.

[47] D. Maynau, *DOLO suite of programs*, Université Paul Sabatier Toulouse, France, 2010.

[48] N. Ben Amor, D. Maynau, *Chem. Phys. Lett.*, 1998, **286**, 211.